RSC Advances

PAPER

View Article Online
View Journal | View Issue

Cite this: *RSC Adv.*, 2015, **5**, 77288

Highly flexible and transparent metal grids made of metal nanowire networks†

Chulhee Lee,[a] Chuntae Kim,[a] Minseok Jeong,[b] Jeonghyo Kim,[c] Jaewook Lee,[d] Jin-Woo Oh,[a] Jaebeom Lee,[c] Soo Hyung Kim,[a] Simon S. Park[d] and Jong-Man Kim*[a]

Received 22nd July 2015
Accepted 3rd September 2015

DOI: 10.1039/c5ra14513a

www.rsc.org/advances

This work reports a new flexible transparent conductive electrode architecture based on solution-processed silver nanowire percolation metal grids (AgNW MGs). The AgNW MGs are stably fabricated by a well-established wet coating method and subsequent selective chemical etching of the AgNWs. The fabricated AgNW MGs exhibit good optoelectronic performance with sheet resistances of 9.9 Ω sq^{-1} and 14.7 Ω sq^{-1} at transmittances of 84.7% and 88.7%, respectively. The integration of percolated NW networks into the micro-grid structures also enables reproducible fabrication and controllable and reversible performance. The electrical robustness is greatly improved by incorporating a conductive polymer over-coating.

Introduction

The mechanical compliance of transparent conductive electrodes (TCEs) is one of the most important requirements for numerous emerging optoelectronic devices, including flexible displays, solar cells, and touch screens. To date, indium tin oxide (ITO) has been most widely used as a transparent conductive material in many applications due to the superior electrical and optical performance. However, the inherently brittle ceramic properties of ITO critically hinder its practical use in flexible platforms.[1] In addition, the electrical conductivity of ITO deposited on plastic substrates is often insufficient for such specific applications.[2,3] In response to the increased demand for functional flexible optoelectronic devices, extensive studies have been done to develop alternatives that can overcome the limitations of ITO-based TCEs. Recently, flexible TCEs have been developed using two main electrical network architectures: 'random networks'[2–24] and 'regular (periodic) networks'.[25–37]

Flexible TCEs with random electrical networks are mainly based on irregularly percolated networks of conductive nanomaterials, such as silver nanowires (AgNWs),[2–16] copper nanowires (CuNWs),[17–19] carbon nanotubes (CNTs),[20–23] and a hybrid of AgNWs and CNTs.[24] In these approaches, the percolated networks were easily prepared by simple solution-based coating methods, including drop-casting,[2–4] filtration,[5,6,18–24] spray-coating,[7–9,19] spin-coating,[10–12] Meyer rod coating,[13–15,17] and brush painting.[16] In spite of the desirable solution-processability, TCEs with randomly percolated networks have some drawbacks. One is a lack of uniformity of the electrical and optical performance due to the random distributions of conductive nanomaterials and irregular pitches between them. Second, it is difficult to ensure reproducible fabrication. The problems are intensified with low-density percolated networks, which are crucial for achieving high optical transparency.

Flexible TCEs with regular electrical networks mainly consist of periodic metal grids (MGs). Both fabrication and performance of such TCEs can potentially be uniform and reproducible, because periodic MGs can be stably fabricated without appreciable uncertainty by optimizing the process. In addition, the electrical and optical performance are highly programmable and predictable, because design layouts of MGs can be easily and precisely controlled. Thin-film MGs have been prepared by well-stabilized techniques, including chemical etching of thin-film metals,[25,26] metal lift-off,[27–29] and metal transfer printing.[30,31] However, these methods involve a high-vacuum process, such as sputtering or evaporation of metal, which results in complex and expensive fabrication. Non-vacuum

[a]*Department of Nano Fusion Technology, BK21 Plus Nano Convergence Technology Division, Pusan National University, Busan 609-735, South Korea. E-mail: jongkim@pusan.ac.kr*

[b]*Department of Nanomechatronics Engineering, Pusan National University, Busan 609-735, South Korea*

[c]*Department of Cogno-Mechatronics Engineering, Pusan National University, Busan 609-735, South Korea*

[d]*Department of Mechanical and Manufacturing Engineering, University of Calgary, Calgary, Alberta T2N 1N4, Canada*

† Electronic supplementary information (ESI) available: AFM images and average surface roughness of AgNW films as a function of pressing force (Fig. S1), transmittance spectra (400 nm to 800 nm) of AgNW MGs with different grid-to-grid pitch ranging from 100 μm to 600 μm and a step of 100 μm (Fig. S2), sheet resistances and transmittances (550 nm) of AgNW MGs processed with different chemical etching time with and without PEDOT:PSS over-coating (Fig. S3), transmittance spectrum (400 nm to 800 nm) of spray-coated PEDOT:PSS layer (Fig. S4), transmittance spectra (400 nm to 800 nm) of AgNW MGs processed with different chemical etching time with and without PEDOT:PSS over-coating (Fig. S5), SEM images of AgNW MG after repetitive bending tests for up to 500 cycles (Fig. S6). See DOI: 10.1039/c5ra14513a

methods include jet printing[32–36] and selective laser sintering[37] of metallic ink. Although simple fabrication is achievable, these vacuum-free approaches may suffer from long processing time due to the direct writing nature and difficulty in precision control of the critical dimensions of MGs. Additionally, the methods require specific equipment. Some unconventional methods such as capillary force-mediated assembly[38] and contact printing[39] have been introduced to assemble conductive nanomaterials into arrayed structures by aligning them in a precise and controllable manner. However, they would be unsuitable for fabricating large-area metal grids mainly due to quite cumbersome alignment process.

This work presents solution-processable and potentially reproducible fabrication method for metal grids made of AgNW percolation networks for flexible TCEs. Wet coating of the AgNWs and subsequent chemical etching with a photolithographically defined polymeric etching mask make it possible to synergistically combine the desirable features of both 'random network' and 'regular network' approaches. The advantages of the proposed method possesses are (1) simple and low-cost fabrication due to the solution-processability without high-vacuum or other specific equipment; (2) considerable uniformity in both fabrication and performance due to the regular geometries of MGs; (3) reproducible fabrication based on the integration of well-established processes; and (4) facile controllability of the optoelectronic performance by new mask designs and time-controlled chemical etching of the AgNWs.

Experimental

Synthesis of AgNWs

AgNWs were synthesized using a $CuCl_2$-mediated polyol process.[40] 10 mL of ethylene glycol (EG; Daejung Chemical & Metal) was heated in an oil bath at 160 °C for 1 h while magnetically stirring at 260 rpm. 40 μL of 4 mM copper(II) chloride ($CuCl_2$; Samchun Chemical) was then added to the heated EG. After 15 min, 3 mL of an EG solution containing 0.4 M silver nitrate ($AgNO_3$; Sigma-Aldrich) and 3 mL of another EG solution containing 0.6 M polyvinyl pyrrolidone (PVP; Alfa Aesar) were injected at a rate of 0.3 mL min^{-1} using a 2-channel syringe pump (Legato 111, KD Scientific). The mixture was continuously heated and stirred for 1 h. The synthesized AgNWs were purified with acetone and isopropyl alcohol (IPA) by centrifuging at 2000 rpm for 20 min. The purifying process was repeated several times to obtain clean AgNWs.

Fabrication of AgNW film

The purified AgNWs were dispersed in IPA solution at a concentration of ~8.5 mg mL^{-1}. The AgNW solution was sprayed onto a polyethylene terephthalate (PET) substrate (26 mm (W) × 38 mm (L) × 1 mm (T)) using a commercial airbrush (Shine 3, Sparmax) with a nozzle diameter of 0.3 mm. The spray-coating process was conducted on a hotplate at 95 °C to enhance the evaporation rate of the solvent (IPA). During the process, the nozzle-to-substrate distance and spraying pressure were fixed at ~15 cm and 0.2 MPa, respectively. The as-prepared AgNW film was then thermally treated to reduce the electrical resistance that arises at inter-AgNW junctions by applying a DC voltage of 1.5 V for 35 s instead of high-temperature annealing. Finally, the heat-treated AgNW film was mechanically pressed using a hydraulic material testing system at a normal force of 50 kN for 60 s to achieve both a smooth surface and a further reduction in electrical resistance of the AgNW film.

Fabrication of the AgNW percolation metal grid (AgNW MG)

AgNW grid structures were fabricated by a standard photolithography method and a subsequent chemical etching process. A grid-shaped polymeric etching mask was first defined on the prepared AgNW film. A ~1.4 μm-thick layer of photoresist (PR; AZ5214, MicroChemicals) was spin-coated on the AgNW film at 4000 rpm for 45 s and then baked in a convection oven at 95 °C for 20 min. The sample was then selectively exposed to ultraviolet (UV) light with an intensity of 20 mW cm^{-2} using a commercial mask aligner (MDA-400M, Midas System). The UV-exposed area was developed in a developer (AZ 300 MIF, Clariant) at room temperature for 150 s. Prior to chemical etching, the sample was further baked on a hotplate at 135 °C for 90 s to improve the etching selectivity of the PR etching mask. Using the mask, the AgNW percolation network between grid lines was chemically etched in 9 M nitric acid (HNO_3) solution at room temperature. The processed sample was carefully rinsed in deionized (DI) water and then dried by nitrogen (N_2) flow.

A thin over-coating layer was conformally deposited on the prepared AgNW MG by spraying 1 mL of an aqueous solution of poly(3,4-ethylenedioxythiophene):poly(4-styrenesulfonate) (PEDOT:PSS; Clevios P, Heraeus). The spray-coating process was carried out on hotplate at 95 °C while maintaining a spray distance of ~15 cm and an airbrush pressure of 0.1 MPa.

Characterization

The surface morphology of the fabricated AgNW MG was characterized using an optical microscope (BX60M, Olympus) and a field emission scanning electron microscope (FESEM; S4700, Hitachi). The surface roughness of the AgNW film and a detailed cross-sectional image of the AgNW percolation grid line were observed using an atomic force microscope (AFM; NX10, Park Systems) in non-contact mode. The sheet resistance was characterized by measuring the electrical resistance of the square-shaped AgNW MG structure (W/L = 1) using a two-terminal method.[25,37,41,42] The electrical resistance was measured using a digital multimeter (U1273A, Agilent). The optical transmittance was measured using a UV-visible spectrophotometer (Evolution 220, Thermo Scientific) at wavelengths ranging from 400 nm to 800 nm. The transmittance of the substrate was excluded.

Adhesion test

The adhesion strength of the AgNW MG to a substrate was tested up to ten times using commercial adhesive tape (no. 810, 3M). The tape was firmly pressed onto the sample surface with

finger pressure, and change in the sheet resistance was recorded after peeling off the tape.

Bending test

To investigate mechanical stability, a bending test was performed by applying uniform bending strain to the sample at a loading speed of 25 mm min^{-1} using a commercial tensile tester (JSV-H100, JISC) interfaced to a computer with an RS-232 data cable. The electrical resistances in the loading and unloading states were measured upon testing, and averaged from five repetitive tests for each sample. A cyclic bending test was conducted for up to 500 cycles at a loading speed of 60 mm min^{-1} with a minimum bending radius of 5 mm. The corresponding sheet resistance was measured every 100 cycles.

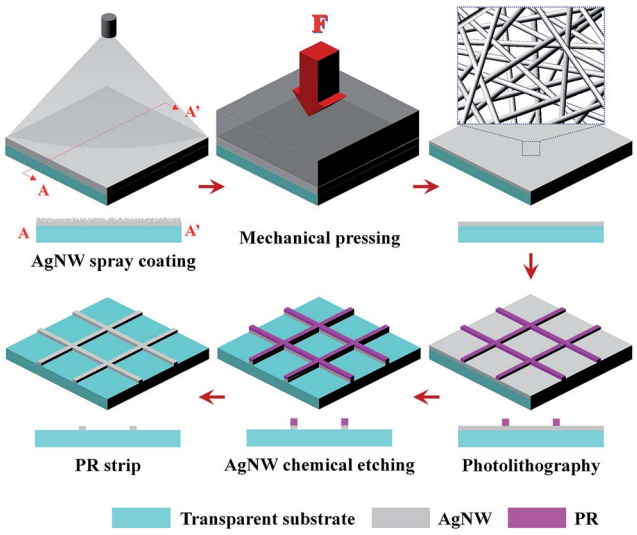

Fig. 1 Schematic illustration of fabrication process for AgNW MGs.

Results and discussion

The flexible AgNW MG was fabricated by selective chemical etching of AgNW film with a PR etching mask formed by a photolithography process, as schematically illustrated in Fig. 1. The well-established photolithography and chemical etching methods enable preparation of AgNW percolation MGs in a simple and potentially scalable manner. The PR etching mask should be stably defined without defects to fabricate definite grid structures through subsequent chemical etching over a large area. Smooth surface morphology of the AgNW film is required, because both the patterning accuracy and critical dimension (CD) uniformity in the photolithographic process strongly depend on the surface roughness of the substrate.

Facile mechanical pressing can efficiently enhance both the surface roughness and electrical conductivity of the as-coated AgNW film, which usually has roughened surface morphology.[43] The average roughness (R_a) of AgNW film was gradually decreased with increasing the normal pressing force, resulting in R_a = 0.37 μm at 50 kN (see Fig. S1†). The sheet resistance of AgNW film pressed at 50 kN was as low as 0.2 Ω sq^{-1}.

The PR etching mask formed on the as-coated AgNW film was partially unclear because of the high surface roughness (R_a = 0.81 μm), as shown in Fig. 2a. This would severely affect the electrical performance and uniformity of the AgNW MG by totally breaking several grid lines (current paths) or locally reducing the AgNW densities after chemical etching. On the other hand, it was found that the PR etching mask can be uniformly defined on AgNW film pressed at 50 kN due to the smooth surface morphology enabled by the mechanical pressing, as shown in Fig. 2b.

Fig. 3a clearly shows the flexible and transparent nature of the fabricated AgNW MG. With the optimized process conditions, the AgNW percolation grid structures were uniformly

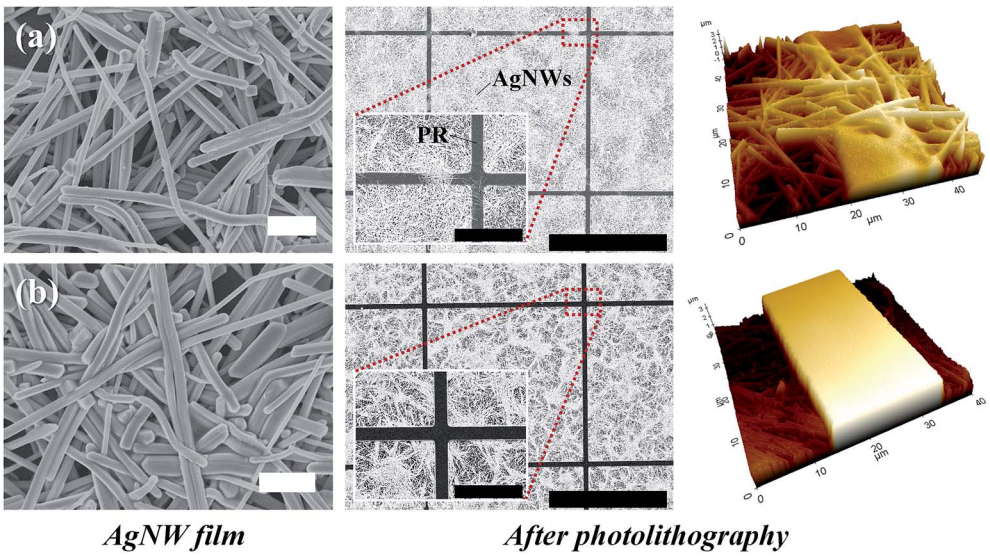

Fig. 2 Effect of mechanical pressing on pattering stability in photolithographic process. SEM and AFM images of AgNW films before and after photolithography process (a) without and (b) with mechanical pressing (50 kN) (white scale bars: 2 μm; black scale bars: 500 μm, 100 μm (inset)).

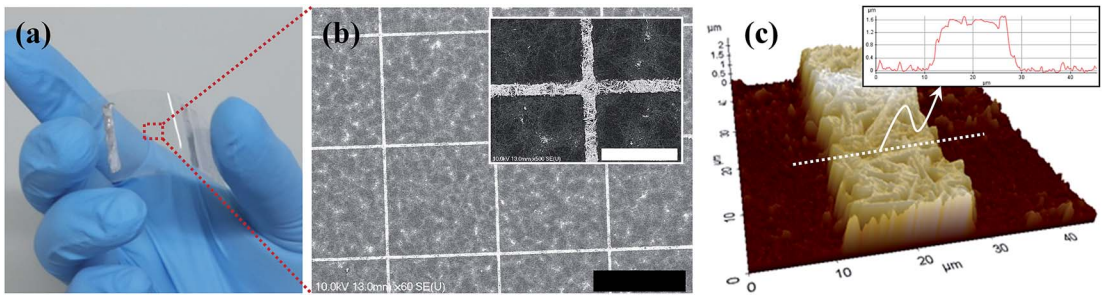

Fig. 3 Fabrication results. (a) Digital image and (b) SEM images of the fabricated AgNW MG (black scale bar: 500 μm; white scale bar: 100 μm). (c) 3D and cross-sectional AFM images of the grid-line.

fabricated without structural uncertainties, as shown in the SEM images in Fig. 3b. The 3D and cross-sectional AFM profiles in Fig. 3c indicate that the thickness and width of the fabricated AgNW grid line are ~1.4 μm and ~20 μm, respectively.

Due to the regular grid architecture of the AgNW MG, the optoelectronic performance can be easily controlled by varying several geometrical parameters, such as the height and width of the grid line and the grid-to-grid pitch. Fig. 4 shows the electrical and optical properties of the fabricated flexible AgNW MGs as a function of pitch (100 μm to 600 μm with a step of 100 μm) and a fixed grid height and width of ~1.4 μm and ~20 μm, respectively. The sheet resistance (R_s) of the AgNW MG increased with the pitch, as shown in Fig. 4a. The results indicate that sheet resistance as low as 22 Ω sq^{-1} is obtainable for a pitch of up to 600 μm, which is comparable or superior to conventional ITO thin-films.[25,43]

Fig. 4b shows the optical transmittance (T) measured at a wavelength of 550 nm for each AgNW MG with different pitch. Full transmittance spectra (400 nm to 800 nm) are also provided in Fig. S2.† Digital images of each sample on a logo of our institution are displayed in the inset of Fig. 4b. The transmittance was also gradually increased to 86.3% (pitch = 400 μm) with increasing pitch, and eventually saturating at ~88% (pitch ≥ 500 μm), as shown in Fig. 4b. A low sheet resistance of 14.7 Ω sq^{-1} and high optical transmittance of 88.2% (at 550 nm) were

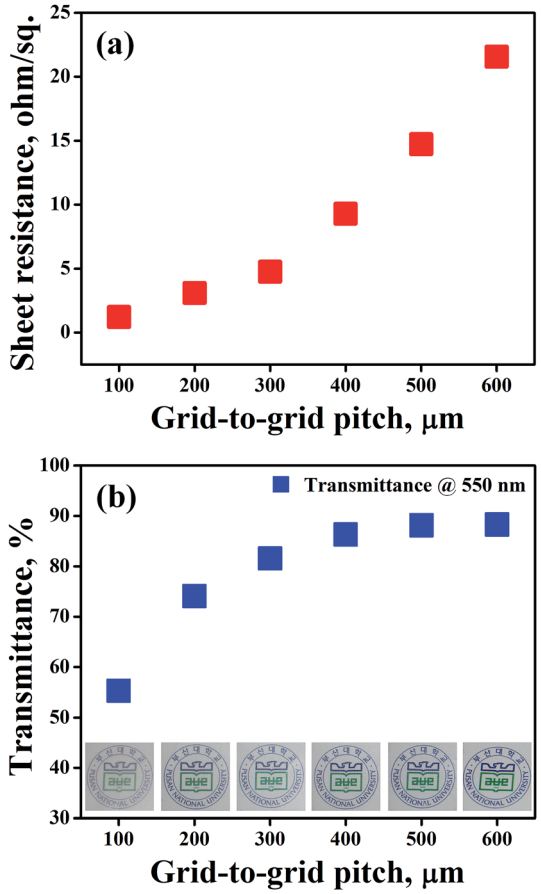

Fig. 4 The optoelectronic performance of AgNW MGs with different grid-to-grid pitch of 100 μm to 600 μm with a step of 100 μm. (a) Sheet resistances and (b) transmittances at 550 nm wavelength of each AgNW MG (inset: digital images of each AgNW MG placed on a logo of our institution).

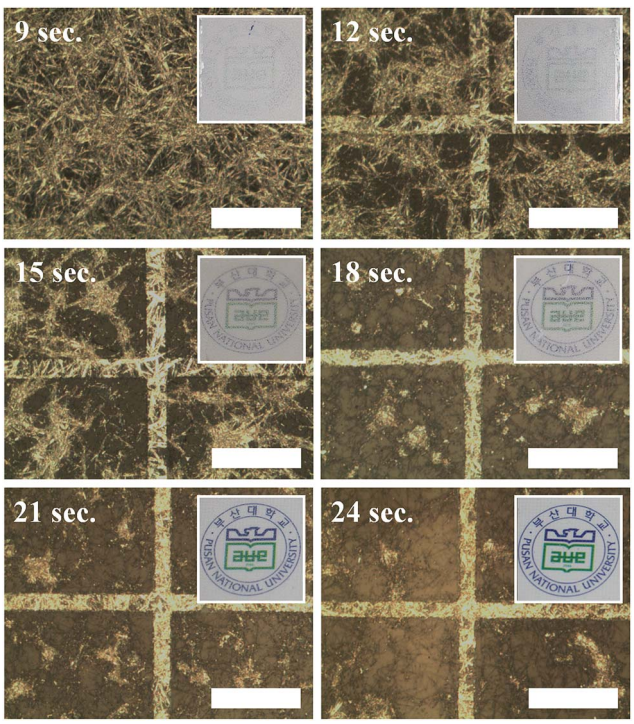

Fig. 5 Microscope images of AgNW MGs prepared with different etching times of 0 s to 24 s with a step of 3 s (scale bars: 200 μm; inset: digital images of each AgNW MG placed on a logo of our institution).

simultaneously achieved with the AgNW MG (pitch = 500 μm). This clearly suggests that the proposed approach is fairly useful for obtaining high-performance flexible TCEs.

Fig. 5 shows microscope images of AgNW MGs (pitch = 500 μm) processed with different chemical etching time (9 s to 24 s with a step of 3 s). The AgNW grid structures are clearer with increasing etching time (inset). This is due to the fact that the AgNW percolation network between grid lines (window area) becomes less dense as the chemical etching process progresses.

Fig. 6a shows the sheet resistance of AgNW MGs as a function of chemical etching time, and Fig. 6b shows the optical transmittance at a wavelength of 550 nm. Although a slight increase in the sheet resistance was observed, a low sheet resistance of <1 Ω sq^{-1} was maintained for up to 15 s. This means that the AgNW density in the window area is still high enough to ensure high electrical conductivity.

The sheet resistance was suddenly increased to 2.1 Ω sq^{-1} at 18 s, and linearly proportional to the etching time with a steep slope after this point, as shown in Fig. 6a. In addition, a sudden increase in the optical transmittance was observed at 18 s (T = 54.9%) due to considerable reduction of the AgNW density in the window area. Fig. 6b also suggests that high optical transmittance over 80% can be achieved when the etching time exceeds 18 s. The results imply that the optoelectronic performance of the AgNW MGs can also be precisely optimized by controlling AgNW density in the window area by varying the etching time without change in mask designs. For example, a low sheet resistance of 9.9 Ω sq^{-1} and high transmittance of 84.7% were obtained at 21 s.

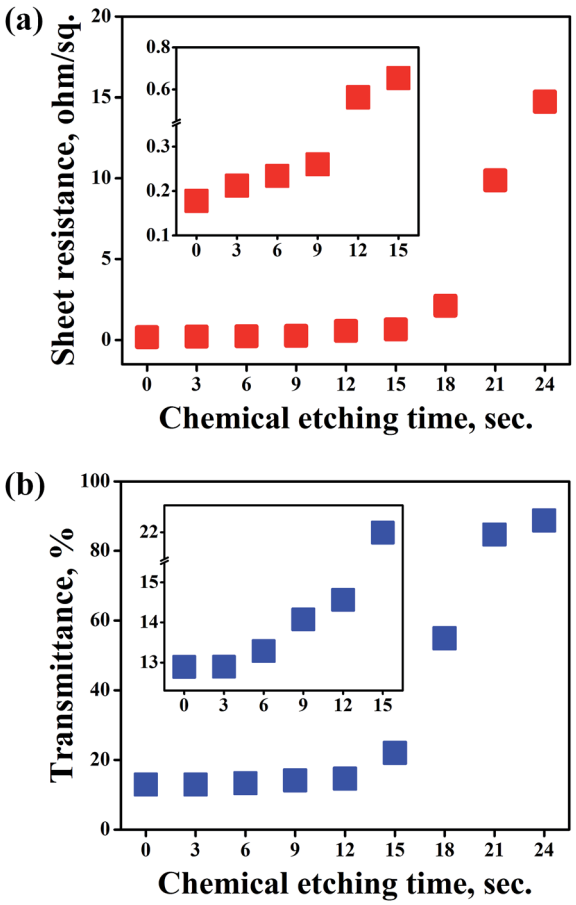

Fig. 6 The optoelectronic performance of AgNW MGs with different chemical etching time. (a) Sheet resistances and (b) transmittances at 550 nm wavelength for each AgNW MG.

To promote the adhesion between the AgNWs and substrate, a thin conductive polymer layer (PEDOT:PSS) was deposited on the fabricated AgNW MGs.[44] Fig. 7 shows SEM image of the AgNW MG after PEDOT:PSS over-coating, which indicates that the PEDOT:PSS conformally covered the entire sample surface. The over-coating of conductive polymer led to decreases in both the sheet resistance and the transmittance of AgNW MGs, depending on the electrical and optical properties.

Fig. 8a and b respectively show the decrease in the sheet resistance and transmittance at 550 nm of AgNW MGs processed with different etching time after PEDOT:PSS coating. The measured sheet resistances and transmittances are also provided in Fig. S3.†

The sheet resistances of all PEDOT:PSS-coated samples were improved compared to before coating, as shown in Fig. 8a. This originates from two factors: (1) the AgNWs in the network could be tightened against each other after coating, resulting in reduction of the contact resistance at the junctions; and (2) isolated AgNWs could be electrically connected with the conductive PEDOT:PSS layer (R_s = 2.1 MΩ sq^{-1}). The PEDOT:PSS over-coating on the sheet resistance was the most significant at 21 s of etching, showing a decrease of 3.2 Ω sq^{-1}. This means that AgNWs remaining in the window area play a great role in producing additional current paths by incorporating into the conductive PEDOT:PSS layer.

Although the optical transmittance of PET substrate was degraded by ~5% (at 550 nm) after PEDOT:PSS coating (see Fig. S4†), the decrease in the transmittances of the AgNW MGs was relatively insignificant (<0.7% at 550 nm) for up to 12 s of etching, even after PEDOT:PSS coating. This implies that the transmittance for this range of etching time is dominated mainly by a high-density AgNW network in the window area rather than the PEDOT:PSS layer. After 18 s, the decrease in the transmittances was maintained at ~5% based on optical properties of the PEDOT:PSS layer, as shown in Fig. 8b. The corresponding transmittance spectra (400 nm to 800 nm) are also presented in Fig. S5.†

The results suggest that AgNW density optimization in the window area with time-controlled etching enables further

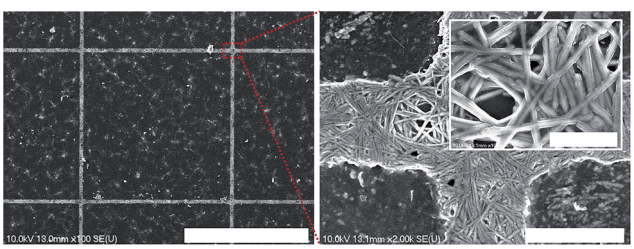

Fig. 7 SEM images of AgNW MG coated with the PEDOT:PSS layer (scale bars: 500 μm (left), 20 μm (right), 5 μm (inset in right)).

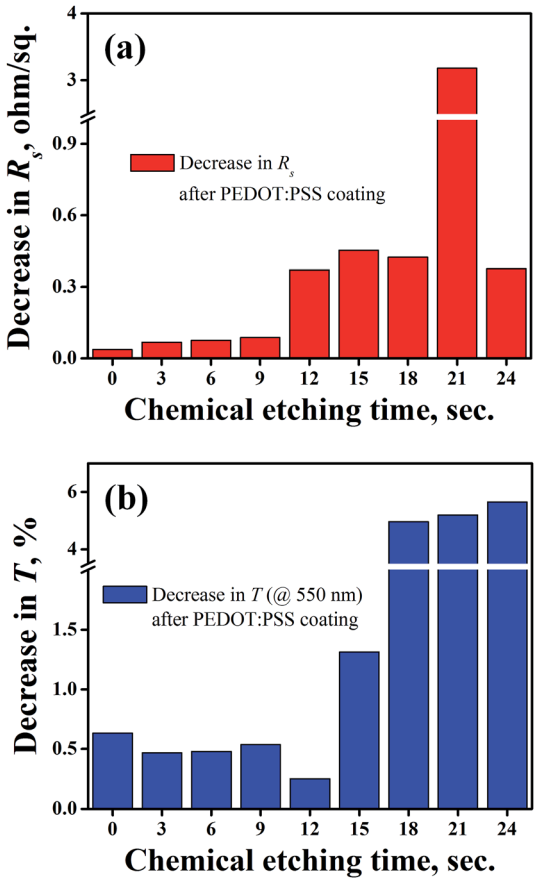

Fig. 8 Effect of PEDOT:PSS over-coating on optoelectronic performance of AgNW MGs. (a) Decrease in sheet resistance and (b) in transmittance at 550 nm wavelength of AgNW MGs with different chemical etching time after PEDOT:PSS coating.

improvement of the electrical performance of AgNW MGs after integration with the conductive over-coating layer while maintaining predictable optical transmittance. For example, the AgNW MG processed for 21 s showed a sheet resistance of 6.7 Ω sq^{-1} and a transmittance of 79.5% at 550 nm after PEDOT:PSS coating.

The effect of the PEDOT:PSS over-coating on adhesion between the AgNWs and substrate was examined by a tape test. Fig. 9a shows the normalized sheet resistances of AgNW MGs with and without PEDOT:PSS over-coating as a function of the number of tape tests. The sheet resistance of the AgNW MG without a PEDOT:PSS over-coating was largely increased (normalized $R_s = \sim 3.9$) after only one cycle of tape test, and it eventually could not be measured after the second cycle due to severe loss of current paths. In contrast, the sheet resistance of the PEDOT:PSS-coated AgNW MG was almost constant with a negligible change of <1%, even after 10 cycles of tape tests. This clearly indicates greatly improved adhesion, as shown in Fig. 9a.

Fig. 9b shows the normalized resistances of AgNW MGs with and without the PEDOT:PSS over-coating in response to bending deformation with a bending radius (R_b) of 5 mm. Upon bending, the resistance of the AgNW MG without the PEDOT:PSS over-coating was increased by ~18% due to loss of current paths in the stress-concentrated regions. However, the increase in the resistance was much alleviated to ~5.2% after PEDOT:PSS coating. When released to 0% bending, the resistance of the AgNW MG without the PEDOT:PSS over-coating almost recovered to the initial value with a minimal increase of ~1.7%. The excellent reversibility is facilitated by the percolated NW network, and it is one of the most desirable properties for numerous flexible electronics applications.

Importantly, the reversibility of the AgNW MG was further improved (~1.7% to ~0.9%) after PEDOT:PSS coating, as shown in Fig. 9b. The electrical performance of the PEDOT:PSS-coated AgNW MG was stable without significant change, even under repetitive bending deformations (at $R_b = 5$ mm) for up to 500 cycles, as shown in Fig. 9c. This originates from the fact that no significant morphological changes were found on the AgNW MG undergone the cyclic bending tests, as shown in Fig. S6.† The results show that the PEDOT:PSS over-coating layer is highly effective for preventing severe structural deformation of the AgNW percolation network during bending, resulting in improvement of the electrical robustness of the AgNW MGs.

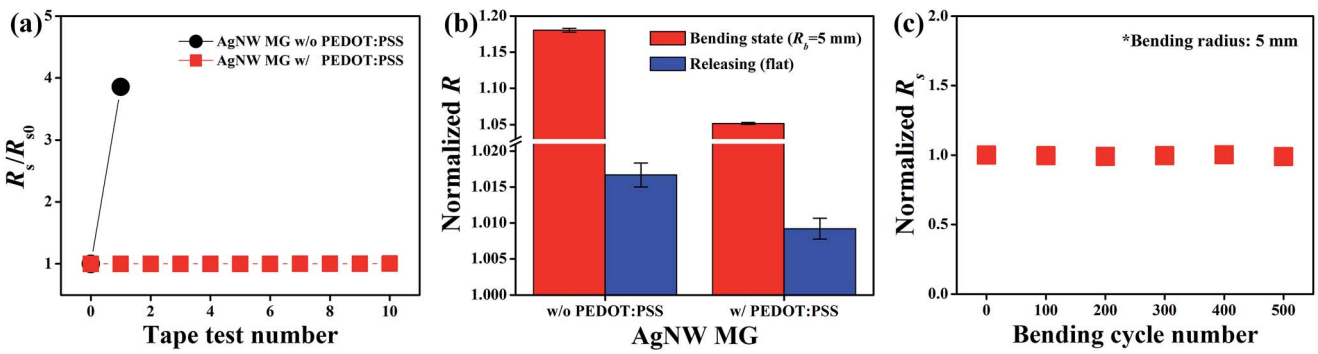

Fig. 9 Mechanical and electrical robustness of PEDOT:PSS-coated AgNW MG. (a) Normalized sheet resistance as a function of tape test number (up to ten times). (b) Normalized resistances in bent (bending radius (R_b): 5 mm) and released (flat) states. (c) Normalized sheet resistance under repetitive bending tests for up to 500 cycles at $R_b = 5$ mm.

Conclusions

In conclusion, we have developed a new class of flexible TCEs based on metal grids made of AgNW percolation networks (AgNW MGs). A simple combination of spray-coating and subsequent selective chemical etching of the AgNWs enabled low-cost and reproducible fabrication, which could potentially lead to high performance uniformity. The electrical and optical properties could be systematically controlled in two ways: (1) new mask designs and (2) time-controlled chemical etching of AgNWs without changing the mask designs, which facilitated more precise optimization of the optoelectronic performance. The fabricated AgNW MGs exhibited sheet resistances of 9.9 Ω sq^{-1} and 14.7 Ω sq^{-1} with transmittances of 84.7% and 88.7%, respectively. The electrical robustness of the AgNW MGs was considerably improved after conductive PEDOT:PSS overcoating, and superior bendability and reversibility were achieved. The optoelectronic performance was further optimized through density control of the AgNWs (in the window area) and subsequent PEDOT:PSS coating by controlling the effective current paths. We believe that the AgNW MGs can greatly contribute to the development of emerging flexible electronics due to advantages such as good performance, facile performance controllability, and electrical robustness and reversibility under bending deformation.

Acknowledgements

This research was supported by Basic Science Research Program (No. 2015R1A2A2A01004038) and the Civil & Military Technology Cooperation Program (No. 2013M3C1A9055407) through the National Research Foundation of Korea (NRF) funded by the Ministry of Science, ICT & Future Planning.

Notes and references

1 D. S. Hecht, L. Hu and G. Irvin, *Adv. Mater.*, 2011, **23**, 1482.
2 L. Li, Z. Yu, W. Hu, C.-H. Chang, Q. Chen and Q. Pei, *Adv. Mater.*, 2011, **23**, 5563.
3 Z. Yu, L. Li, Q. Zhang, W. Hu and Q. Pei, *Adv. Mater.*, 2011, **23**, 4453.
4 R. Chen, S. R. Das, C. Jeong, M. R. Khan, D. B. Janes and M. A. Alam, *Adv. Funct. Mater.*, 2013, **23**, 5150.
5 J. Lee, P. Lee, H. Lee, D. Lee, S. S. Lee and S. H. Ko, *Nanoscale*, 2012, **4**, 6408.
6 M. S. Miller, J. C. O'Kane, A. Niec, R. S. Carmichael and T. B. Carmichael, *ACS Appl. Mater. Interfaces*, 2013, **5**, 10165.
7 B. Hwang, H.-A.-S. Shin, T. Kim, Y.-C. Joo and S. M. Han, *Small*, 2014, **10**, 3397.
8 L. Yang, T. Zhang, H. Zhou, S. C. Price, B. J. Wiley and W. You, *ACS Appl. Mater. Interfaces*, 2011, **3**, 4075.
9 X. He, R. He, A. Liu, X. Chen, Z. Zhao, S. Feng, N. Chen and M. Zhang, *J. Mater. Chem. C*, 2014, **2**, 9737.
10 Y. Liu, Q. Chang and L. Huang, *J. Mater. Chem. C*, 2013, **1**, 2970.
11 S. Nam, M. Song, D.-H. Kim, B. Cho, H. M. Lee, J.-D. Kwon, S.-G. Park, K.-S. Nam, Y. Jeong, S.-H. Kwon, Y. C. Park, S.-H. Jin, J.-W. Kang and C. S. Kim, *Sci. Rep.*, 2014, **4**, 4788.
12 M. Song, D. S. You, K. Lim, S. Park, S. Jung, C. S. Kim, D.-H. Kim, D.-G. Kim, J.-K. Kim, J. Park, Y.-C. Kang, J. Heo, S.-H. Jin, J. H. Park and J.-W. Kang, *Adv. Funct. Mater.*, 2013, **23**, 4177.
13 J. Lee, P. Lee, H. B. Lee, S. Hong, I. Lee, J. Yeo, S. S. Lee, T.-S. Kim, D. Lee and S. H. Ko, *Adv. Funct. Mater.*, 2013, **23**, 4171.
14 C.-H. Liu and X. Yu, *Nanoscale Res. Lett.*, 2011, **6**, 75.
15 H. H. Khaligh and I. A. Goldthorpe, *Nanoscale Res. Lett.*, 2014, **9**, 310.
16 J.-H. Lee, H.-S. Shin, Y.-J. Noh, S.-I. Na and H.-K. Kim, *Sol. Energy Mater. Sol. Cells*, 2013, **114**, 15.
17 A. R. Rathmell and B. J. Wiley, *Adv. Mater.*, 2011, **23**, 4798.
18 H. Guo, N. Lin, Y. Chen, Z. Wang, Q. Xie, T. Zheng, N. Gao, S. Li, J. Kang, D. Cai and D.-L. Peng, *Sci. Rep.*, 2013, **3**, 2323.
19 H.-G. Im, S.-H. Jung, J. Jin, D. Lee, J. Lee, D. Lee, J.-Y. Lee, I.-D. Kim and B.-S. Bae, *ACS Nano*, 2014, **8**, 10973.
20 Z. Wu, Z. Chen, X. Du, J. M. Logan, J. Sippel, M. Nikolou, K. Kamaras, J. R. Reynolds, D. B. Tanner, A. F. Hebard and A. G. Rinzler, *Science*, 2004, **305**, 1273.
21 D. Zhang, K. Ryu, X. Liu, E. Polikarpov, J. Ly, M. E. Tompson and C. Zhou, *Nano Lett.*, 2006, **6**, 1880.
22 J. Ge, G. Cheng and L. Chen, *Nanoscale*, 2011, **3**, 3084.
23 A. Kaskela, A. G. Nasibulin, M. Y. Timmermans, B. Aitchison, A. Papadimitratos, Y. Tian, Z. Zhu, H. Jiang, D. P. Brown, A. Zakhidov and E. I. Kauppinen, *Nano Lett.*, 2010, **10**, 4349.
24 J. Lee, J. Y. Woo, J. T. Kim, B. Y. Lee and C.-S. Han, *ACS Appl. Mater. Interfaces*, 2014, **6**, 10974.
25 Y. Zhu, Z. Sun, Z. Yan, Z. Jin and J. M. Tour, *ACS Nano*, 2011, **5**, 6472.
26 J. H. Park, D. Y. Lee, Y.-H. Kim, J. K. Kim, J. H. Lee, J. H. Park, T.-W. Lee and J. H. Cho, *ACS Appl. Mater. Interfaces*, 2014, **6**, 12380.
27 T. Qiu, B. Luo, M. Liang, J. Ning, B. Wang, X. Li and L. Zhi, *Carbon*, 2015, **81**, 232.
28 P. Dong, Y. Zhu, J. Zhang, C. Peng, Z. Yan, L. Li, Z. Peng, G. Ruan, W. Xiao, H. Lin, J. M. Tour and J. Lou, *J. Phys. Chem. C*, 2014, **118**, 25863.
29 M.-G. Kang and L. J. Guo, *Adv. Mater.*, 2007, **19**, 1391.
30 M.-G. Kang, M.-S. Kim, J. Kim and L. J. Guo, *Adv. Mater.*, 2008, **20**, 4408.
31 M.-G. Kang, H. J. Park, S. H. Ahn and L. J. Guo, *Sol. Energy Mater. Sol. Cells*, 2010, **94**, 1179.
32 J. Park and J. Hwang, *J. Phys. D: Appl. Phys.*, 2014, **47**, 405102.
33 Y. Jang, J. Kim and D. Byun, *J. Phys. D: Appl. Phys.*, 2013, **46**, 155103.
34 B. Seong, H. Yoo, V. D. Nguyen, Y. Jang, C. Ryu and D. Byun, *J. Micromech. Microeng.*, 2014, **24**, 097002.
35 Y. H. Kahng, M.-K. Kim, J.-H. Lee, Y. J. Kim, N. Kim, D.-W. Park and K. Lee, *Sol. Energy Mater. Sol. Cells*, 2014, **124**, 86.
36 B. Murali, D.-G. Kim, J.-W. Kang and J. Kim, *Phys. Status Solidi A*, 2014, **211**, 1801.

37 S. Hong, J. Yeo, G. Kim, D. Kim, H. Lee, J. Kwon, H. Lee, P. Lee and S. H. Ko, *ACS Nano*, 2013, **7**, 5024.
38 X. Zhou, Y. Zhou, J. C. Ku, C. Zhang and C. A. Mirkin, *ACS Nano*, 2014, **8**, 1511.
39 K. Takei, T. Takahashi, J. C. Ho, H. Ko, A. G. Gillies, P. W. Leu, R. S. Fearing and A. Javey, *Nat. Mater.*, 2010, **9**, 821.
40 K. E. Korte, S. E. Skrabalak and Y. Xia, *J. Mater. Chem.*, 2008, **18**, 437.
41 P.-C. Hsu, S. Wang, H. Wu, V. K. Narasimhan, D. Kong, H. R. Lee and Y. Cui, *Nat. Commun.*, 2013, **4**, 2522.
42 A. D. Printz, E. Chan, C. Liong, R. S. Martinez and D. J. Lipomi, *PLoS One*, 2013, **8**, e83939.
43 L. Hu, H. S. Kim, J.-Y. Lee, P. Peumans and Y. Cui, *ACS Nano*, 2010, **4**, 2955.
44 D. Y. Choi, H. W. Kang, H. J. Sung and S. S. Kim, *Nanoscale*, 2013, **5**, 977.